Microbial competition in porous environments can select against rapid biofilm growth

Katharine Z. Coyte[a,b,c,d], Hervé Tabuteau[e], Eamonn A. Gaffney[b], Kevin R. Foster[a,c,1], and William M. Durham[a,f,1]

[a]Department of Zoology, University of Oxford, Oxford OX1 3PS, United Kingdom; [b]Wolfson Centre for Mathematical Biology, University of Oxford, Oxford OX2 6GG, United Kingdom; [c]Oxford Centre for Integrative Systems Biology, University of Oxford, Oxford OX1 3QU, United Kingdom; [d]Computational Biology, Memorial Sloan Kettering Cancer Center, New York, NY 10065; [e]Institut de Physique de Rennes, Université de Rennes 1, 35042 Rennes, France; and [f]Department of Physics and Astronomy, University of Sheffield, Sheffield S3 7RH, United Kingdom

Edited by Howard A. Stone, Princeton University, Princeton, NJ, and approved November 1, 2016 (received for review December 21, 2015)

Microbes often live in dense communities called biofilms, where competition between strains and species is fundamental to both evolution and community function. Although biofilms are commonly found in soil-like porous environments, the study of microbial interactions has largely focused on biofilms growing on flat, planar surfaces. Here, we use microfluidic experiments, mechanistic models, and game theory to study how porous media hydrodynamics can mediate competition between bacterial genotypes. Our experiments reveal a fundamental challenge faced by microbial strains that live in porous environments: cells that rapidly form biofilms tend to block their access to fluid flow and redirect resources to competitors. To understand how these dynamics influence the evolution of bacterial growth rates, we couple a model of flow–biofilm interaction with a game theory analysis. This investigation revealed that hydrodynamic interactions between competing genotypes give rise to an evolutionarily stable growth rate that stands in stark contrast with that observed in typical laboratory experiments: cells within a biofilm can outcompete other genotypes by growing more slowly. Our work reveals that hydrodynamics can profoundly affect how bacteria compete and evolve in porous environments, the habitat where most bacteria live.

bacterial evolution | porous media flow | clogging | game theory | adaptive dynamics

Modern microbiology relies on growing cells in liquid cultures and agar plates. Although these conditions offer high throughput and repeatability, they lack the complex physical and chemical landscapes that microbes experience in their natural environments. This environmental heterogeneity is increasingly recognized to exert a powerful influence on microbial ecology across a wide diversity of habitats, ranging from the ocean to the human gut (1–4). Although advances in sequencing technology now allow us to resolve how the genetic composition of microbial communities changes in response to environmental conditions (5, 6), we often lack a mechanistic understanding of the underlying processes. Novel empirical approaches, which simulate the conditions found in realistic microbial habitats, are needed to understand the strategies that cells use to gain an advantage over their competitors (7).

The overwhelming majority of bacteria live in porous environments between the particles that compose soil, aquifers, and sediments, and cumulatively comprise roughly half of the carbon within living organisms globally (8). Cells in porous environments typically reside in surface attached structures known as biofilms (9), in which diverse bacterial genotypes live under intense competition for limited resources (10, 11). Recent efforts have identified specialized mechanisms that cells use to gain advantage over competing genotypes in biofilms, ranging from the secretion of toxins to polymer production and metabolic regulation (12–18). Whereas genotypic competition is most frequently studied in biofilms growing on simple flat surfaces (19–21), biofilms growing in the interstitial spaces within porous structures face additional constraints. In porous environments, space is much more limited, and biofilm growth tends to attenuate the fluid flow that supplies cells with nutrients and facilitates dispersal.

Biofilms typically reduce the flow through porous environments by orders of magnitude at the Darcy scale (22), a macroscopic scale that measures the flow averaged over many pore spaces. Harnessing this effect, biofilms can be used to limit the transport of pollutants that have leaked into groundwater aquifers and to facilitate the extraction of petroleum from recalcitrant regions of reservoirs (23, 24). However, biofilm-induced clogging also generates unwanted effects: for example, it severely limits the efficiency of porous filtration systems (25) and curtails the rate at which water infiltrates into aquifers (26), exacerbating droughts. Due to its importance, the attenuation of flow by biofilms has long been studied at the Darcy scale (27, 28), and more recent works have sought to resolve how this process, in turn, is mediated by biofilm–hydrodynamic interactions at the microscopic pore scale (29–31). However, it is largely unknown how these interactions influence the ecology and evolution of the bacteria themselves. Here, we combine experiments and models to show that porous media hydrodynamics can dramatically affect the principles of bacterial competition and evolution.

Results

A Conceptual Model to Study Hydrodynamic Interactions Between Competing Biofilms. Bacteria within biofilms tend to form patches of genetically identical cells, even when the cells from which they

Significance

The overwhelming majority of bacteria live in porous environments, like soil, aquifers, and sediments, where they facilitate many important processes. Despite their importance, we understand little about how these complex environments shape the composition of the microbial communities that live within them. Here, we combine two diverse bodies of theory—fluid dynamics and game theory—to shed light on how bacteria evolve in these habitats. We show that bacteria in porous environments face a fundamental dilemma: they rely on flow for nutrients and dispersal; however, as cells grow, they tend to reduce their access to flow. A fast growing strain can, therefore, choke off its own nutrient supply, diverting it instead to competitors. In contrast with classical theory, our results suggest that cells within a biofilm can obtain a competitive advantage by growing more slowly.

Author contributions: K.Z.C., H.T., and W.M.D. designed and performed the microfluidic experiments; K.Z.C., E.A.G., K.R.F., and W.M.D. developed the mathematical models; and K.Z.C., E.A.G., K.R.F., and W.M.D. wrote the paper.

The authors declare no conflict of interest.

This article is a PNAS Direct Submission.

[1]To whom correspondence may be addressed. Email: kevin.foster@zoo.ox.ac.uk or w.m.durham@sheffield.ac.uk.

This article contains supporting information online at www.pnas.org/lookup/suppl/doi:10.1073/pnas.1525228113/-/DCSupplemental.

are founded are initially mixed. This genotypic patchiness occurs because in situ growth, combined with the low mobility of cells within biofilms, means that clone mates tend to remain in close proximity to one another (32, 33). Moreover, genotypic patchiness in biofilms is enhanced by population bottlenecks, which occur more frequently in nutrient-limited conditions, and when biofilms are initiated from a sparse distribution of attached cells (34–36). Based on these observations, we focus here on the competition between localized biofilm "patches" that each comprise a single genotype and assume that competing patches occupy different pore spaces.

To investigate how biofilm growth influences the flow through a porous environment, we calculated the Stokes flow through a representative network of pore spaces that is driven by a difference in pressure at the boundaries (Fig. 1*A* and *Materials and Methods*). The addition of a small impermeable biofilm patch sharply reduces the flow through the pore in which the biofilm resides, while concurrently increasing the flow through neighboring pores (Fig. 1 *B* and *C*). Although the magnitude of this flow diversion depends on the specific geometry of the pore space, this simulation shows that as a biofilm patch proliferates, it tends to decrease its access to flow, while increasing the flow to patches of biofilm that reside along other flow paths. This diversion of flow introduces a way in which biofilms can interact: genotypes inhabiting a porous environment can affect one another via modulating their respective access to flow. This "hydrodynamic interaction" differs from interactions observed in classical biofilm assays, where different genotypes growing together on flat surfaces typically have to be in close proximity to interact, for example, through capturing one another's nutrients or via cell secretions. Rather, here we see that in porous environments, biofilms can influence one another over much larger distances, by either curtailing or increasing one another's ability to capture flow.

Although porous substrates harbor many biofilm patches that can simultaneously perturb one another's flow environment, we idealize this network of interactions as a collection of its constituent pairwise interactions. We then resolve the dynamics of competition between a single pair of biofilm patches, each of which is composed of a different genotype. In this pairwise approximation, the proportion of the total volumetric flow rate, Q_T, that passes each biofilm is a function of the hydrodynamic resistance of both its pore space and that of its competitor, each of which, in turn, is a function of the thicknesses of the biofilms, k_1 and k_2 (Fig. 1 *D* and *E*). In this model, the growth of a biofilm tends to decrease its access to flow and increase the flow past its competitor (Fig. 1*F*). Importantly, our pairwise model captures the dynamics observed in our Stokes flow simulation but is much more tractable and easily parameterized. Flow through a network of pore spaces can be modeled by fixing either the pressure gradient or the flow rate at the boundaries (37), with the former better characterizing flow through natural systems. However, localized biofilm growth in either of these scenarios will produce a flow diversion at the pore scale, as observed in our conceptual model.

Microfluidic Experiments Show That Rapidly Expanding Biofilms Tend to Divert Flow to Biofilms That Increase in Thickness More Slowly. We next developed a microfluidic version of our pairwise flow model to experimentally test how pore-scale hydrodynamics affects the competition between genotypes that form biofilms at different rates (Fig. 2 and Fig. S1). Our experiments used a well-studied *Escherichia coli* experimental system. Specifically, we competed wild-type *E. coli* cells with $\Delta rpoS$ cells. The latter cells lack the ability to produce the sigma factor RpoS and, as a result, form biofilms at a much slower rate than the parental genotype (Fig. 2*G* and Fig. S2, and refs. 38 and 39). The two genotypes were inoculated separately in either arm of the device, each of which represents a pore (Fig. 2 *A* and *B*). One of the pores was irrigated with media mixed with dye, whereas the other was irrigated with clear media, which allowed us to measure the relative proportion of flow passing through each pore by tracking the dye interface downstream of their juncture (*SI Text* and Fig. S1). Control experiments showed that neither the dye nor the fluorescent proteins used to differentially label the strains had an appreciable effect on biofilm formation (Fig. S2).

In porous environments biofilm growth is opposed by flow-induced detachment, which reduces the thickness of biofilms by shearing away cells from its surface (40–42). To simulate different ambient flow conditions in our experiment, and thus the relative amount of detachment, we applied a total flow rate of either $Q_T = 0.1$ mL h^{-1} or $Q_T = 2$ mL h^{-1}. In the low-flow treatment, the rapidly expanding wild-type biofilm increased its pore's hydrodynamic resistance and diverted flow to the neighboring pore space containing the $\Delta rpoS$ biofilm. The reduction in flow experienced by the wild-type biofilm further reduces its detachment, driving a positive-feedback loop that ultimately ends with the $\Delta rpoS$ biofilm capturing nearly all of the flow (Fig. 2 *A*, *C*, and *D*; see *SI Text* for details). In contrast, under the high-flow treatment, the flow-induced detachment is increased so that both genotypes form much thinner biofilms (Fig. 2*E*), which allows both genotypes to maintain access to flow for the entire duration of the experiment (Fig. 2 *B* and *C*). Each treatment was repeated three times, and each yielded the same results at steady state (Fig. S3). Access to flow is essential for biofilms to acquire nutrients and disperse progeny downstream: these results suggest that the strength of the ambient flow places a key limitation on how rapidly a biofilm can expand without diverting its flow supply to genotypes that form thinner biofilms.

A Mathematical Model of Flow–Biofilm Interaction Reveals a Diversity of Competitive Regimes and Enables Prediction of How Cell Dispersal Varies in Experiments. Our microfluidic competition experiments suggest that hydrodynamic interactions between biofilms can profoundly affect genotypic competition. To understand this process better, we next developed a model that couple two competing biofilms with a model of flow, enabling us to explore a much wider range of competitive scenarios. Whereas the two pores in our experiment are strongly coupled, such that flow diverted from one pore is fully absorbed by the other pore, in a network of pores, the strength of the hydrodynamic coupling between two competing biofilms will vary depending on the geometry of the pore space and their relative proximity to one another (Fig. 1 *A*–*C*). To account for this variability, we consider two identical fluid pathways of width $2L$ colonized by biofilms of thickness k_1 and k_2, which are connected in parallel to a channel of width $2M$ that does not contain biofilm (Fig. 1 *E*). The dimensionless parameter $M^* = M/L$ then measures the ability for the two biofilms to influence one another via flow: $M^* = 0$ corresponds to the strong coupling observed in our experiments (which lack a third channel without biofilm), whereas for increasing M^*, flow is more likely to be diverted around the focal biofilms as they proliferate. Importantly, for $M^* > 0$, both biofilms are capable of clogging. This model then provides a tractable way to resolve how changing the strength of the hydrodynamic interaction between two biofilms affects their dynamics, without requiring an explicit representation of the pore structure.

A wide range of physical and biological processes can affect biofilm development (43); however, the thickness of biofilms in flowing environments is chiefly governed by the balance between cell division and flow induced detachment (44, 45). Cell division in biofilms is often confined to a layer at the exterior of the biofilm, where substrates are exposed to nutrients from the

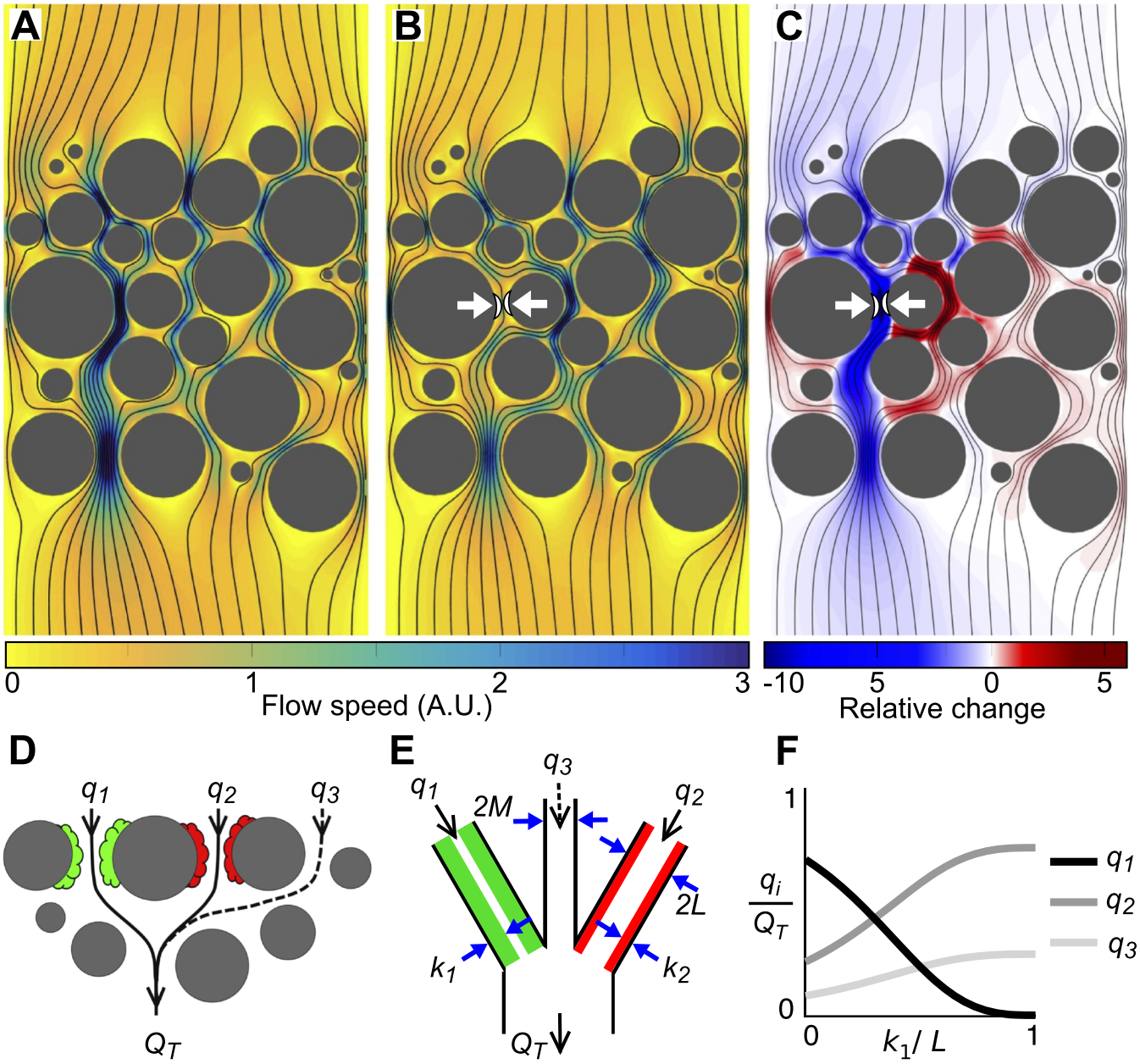

Fig. 1. A growing biofilm tends to decrease its access to flow while increasing the flow to its competitors. (*A*) Viscosity dominates inertia in most porous environments, owing to the relatively small pore spaces (10 μm to 1 mm) and slow fluid velocities (1–1000 μm s^{-1}) (95, 96), which allows flow to be modeled using the Stokes equations. Here, we numerically solved the Stokes equations within a representative 2D porous geometry. Flow is driven by a fixed pressure difference between the top and bottom boundaries, while the left and right boundaries are impermeable (see *Materials and Methods* for further details). Black lines show streamlines, and the color map shows the flow speed in arbitrary units (A.U.). (*B*) The flow field after the addition of a small impermeable patch of biofilm (white arrows). All other parameters of the simulation remained constant. (*C*) The relative change in flow speed measured as $(s_a - s_b)/s_a$, where s_a is the initial flow speed and s_b is the flow speed after the addition of the biofilm patch, shows that the biofilm sharply decreases the flow through the pore in which it resides and increases the flow through neighboring pore spaces. (*D*) A cartoon of two biofilm patches (green and red) that interact hydrodynamically. The proportion of the total flow, Q_T, that moves past each biofilm changes as the biofilms grow and increase the hydrodynamic resistance of their respective pore spaces. A third flow path (dotted line) models the ability for flow to divert around the two competing biofilms. (*E*) Our conceptual model where two biofilms, with thicknesses k_1 and k_2, live along neighboring flow paths of width $2L$ that are connected to a flow path of width $2M$ that does not harbor any biofilm. The proportion of the total volumetric rate flow, Q_T, that passes along each of the three flow paths is calculated using Kirchhoff's laws assuming planar Poiseuille flow in each pore space (*Materials and Methods*). (*F*) Analogous to our Stokes flow simulations, if k_1 increases in thickness the proportion of the total flow rate through its pore space, q_1/Q_T, decreases, while increasing the amount of flow, q_2/Q_T, received by the neighboring biofilm. Here, $k_2/L = 0.3$ and $M/L = 1$.

flow (46, 47). The characteristic thickness, δ, of this metabolically active layer is set by the balance of the diffusion of the substrate into the biofilm with its consumption, which yields the expression $\delta = \sqrt{2c_0 DY/\alpha}$ (48), where c_0 is the substrate's concentration at the outer surface of the biofilm, D is the diffusion coefficient of the substrate in the biofilm, α is the bacterial growth rate, and Y the yield with which cells convert substrate to biomass. The rate at which the biofilm increases in thickness due

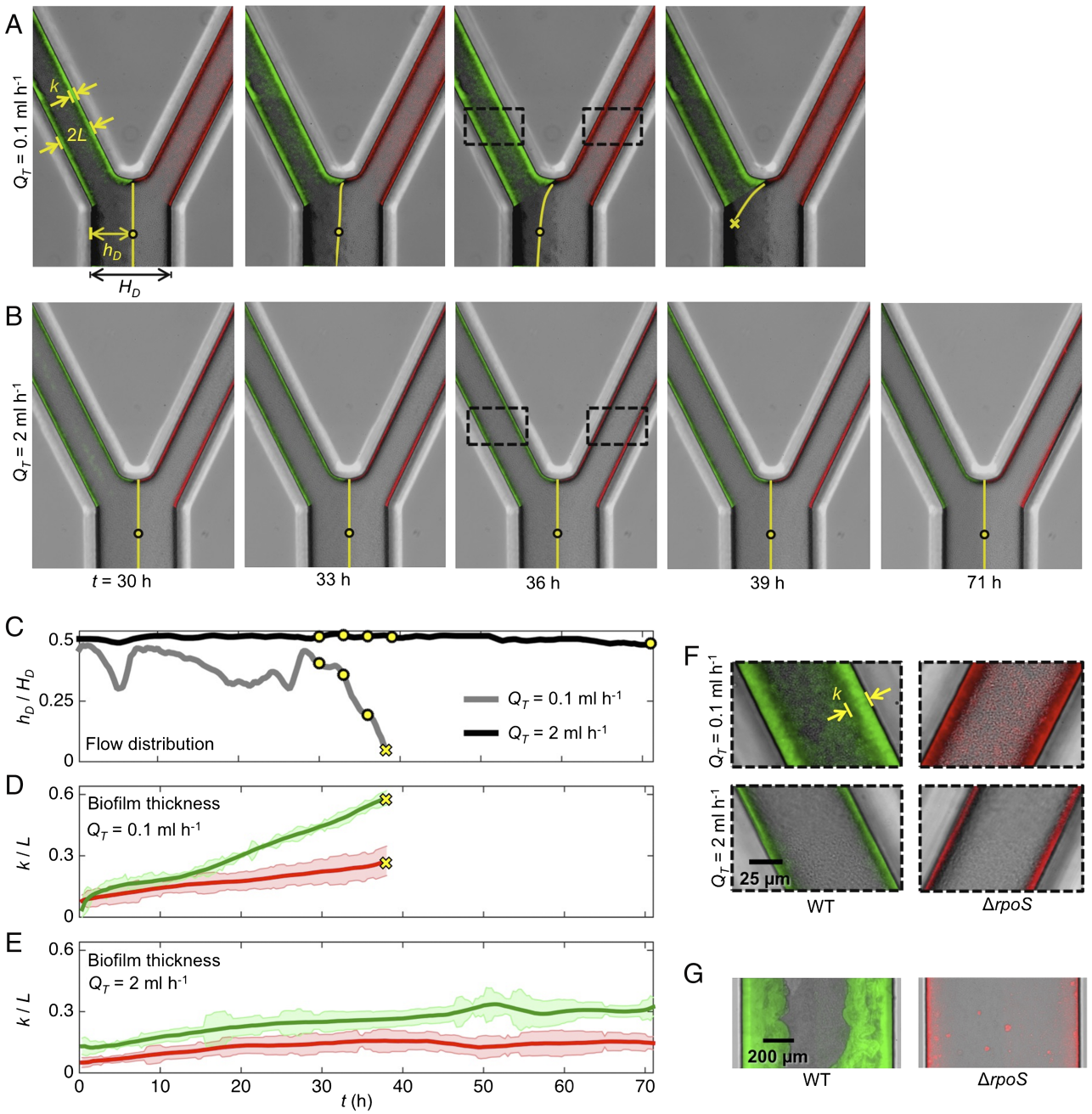

Fig. 2. Microfluidic competition experiments show biofilms that rapidly increase in thickness tend to divert flow to biofilms that expand more slowly. (*A* and *B*) The left pore of each device was seeded with wild-type cells (green), whereas the right pore was inoculated with Δ*rpoS* cells (red). Dyed media flows through the left pore, whereas clear media flows through the right pore. The dye interface downstream of the two pores (yellow line) allows us to dynamically track the proportion of the total flow, Q_T, moving through each pore space (*Materials and Methods*). (*C*) Following the movement of the dye interface (h_D/H_D, yellow circles in *A* and *B*) shows that in the weak-flow treatment (*A*) the wild-type biofilm diverted nearly all its flow supply after 38 h, such that, subsequently, the dye interface was not detectable at the measurement location (*SI Text*). However, in the strong-flow treatment (*B*) both biofilms are able to maintain access to flow for more than 70 h. (*D* and *E*) In the weak-flow treatment the wild-type biofilm (green line) increased in thickness, *k*, faster than the Δ*rpoS*-null biofilm (red line), which was responsible for the diversion of flow. In strong flow, both biofilms were thinner, such that the difference in biofilm thickness between the two strains was smaller. Shaded regions show the standard deviation about the mean (*Materials and Methods*). (*F*) A magnified view of the biofilms shown within the dashed black rectangles in A and B. (*G*) The observation that wild-type biofilms expand at a faster rate than Δ*rpoS* biofilms was confirmed in separate microfluidic experiments that exposed attached cells to much smaller shear stresses than in the competition experiment, which minimized the effect of flow induced detachment (*SI Text*). The upstream arms of the microfluidic devices used in the competition experiments (*A*–*F*) have a width of $2L = 65$ μm and depth of $2B = 75$ μm (Fig. S1).

to cell division is then given by the product of the growth rate, α, and $\min(\delta, k)$, such that $dk/dt = \alpha \min(\delta, k)$, which takes into account that the entire thickness of a biofilm is actively growing when $k < \delta$. Increases in biofilm thickness are countered by the detachment of cells due to mechanical forces exerted at the surface of the biofilm by fluid motion (40). Although the literature contains a diversity of parameterizations to model flow-induced biofilm detachment (see ref. 49 for a comprehensive review), a

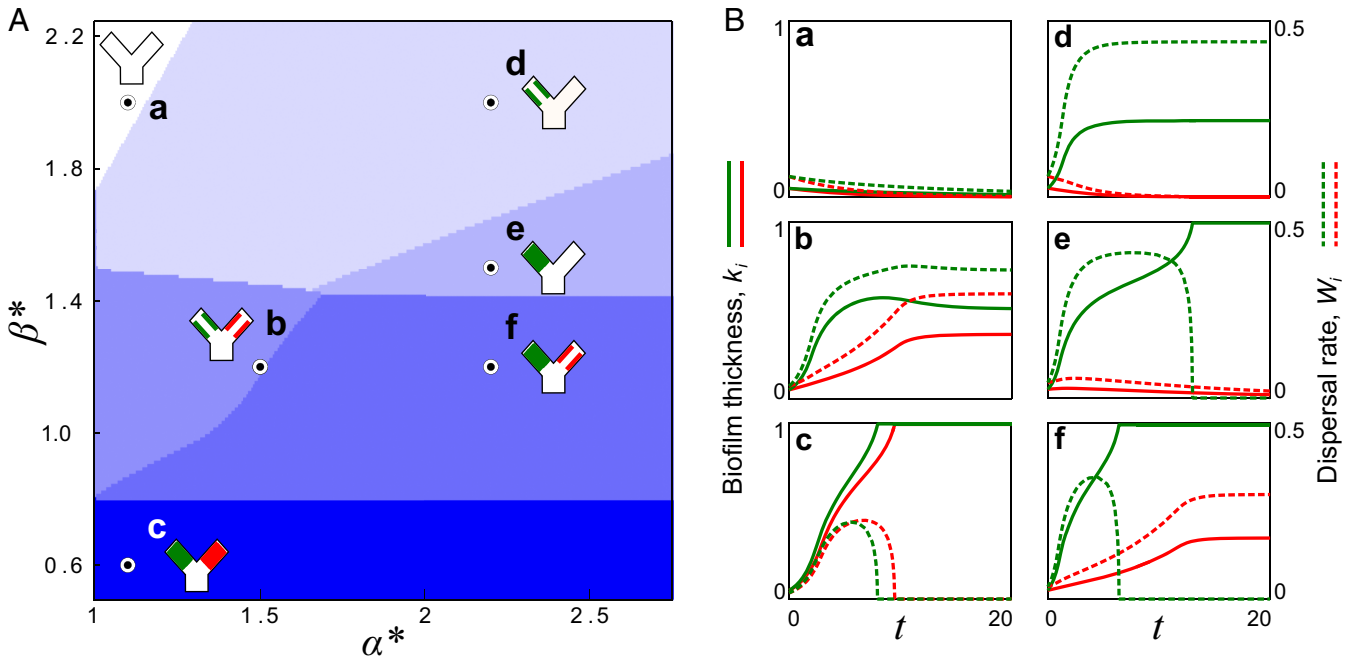

Fig. 3. Diverse ecological regimes emerge from a model of biofilm competition where two strains are coupled by flow. (*A*) The phase space formed by α^*, the growth rate of a fast growing biofilm (green) divided by that of a slower-growing biofilm (red), and β^*, a nondimensional parameter that measures the importance of flow induced biofilm detachment relative to that of biofilm growth, reveals six different regimes at steady state. (*B*, *a*–*f*) Here, we plot the biofilm thicknesses, k_1, k_2 (solid lines), and the dispersal rates, W_1, W_2 (dashed lines), for a representative simulation in each of the regimes (circles in *A*). When a biofilm is fully scoured from the surface ($k_i = 0$) or completely blocks its pore space ($k_i = 1$), its dispersal goes to zero ($W_i = 0$). In contrast, if a biofilm thickness reaches a nontrivial fixed point ($0 < k_i < 1$), it disperses cells downstream at steady state. Here, $M^* = 1, \delta^* = 0.3$. For clarity, we have omitted the third flow path from the cartoons in *A*.

formulation based on the empirical study of ref. 50 is one of the most widely used (45, 51–55) and has been independently confirmed for biofilms growing in porous media (54, 55). Here, the detachment rate is approximated by $dk/dt = -\chi k\tau^{1/2}$, where χ is an empirical parameter with units of $\sqrt{\text{length}/\text{mass}}$ that measures the ability of the biofilm to resist detachment, and τ is the shear stress exerted by the flow on the surface of the biofilm. As such, we model changes in the thickness of biofilm via the superposition of cell-division growth and flow-induced detachment,

$$\frac{dk_i}{dt} = \alpha_i \min(\delta_i, k_i) - \chi k_i \tau^{1/2}, \qquad [1]$$

where $\delta_i = \sqrt{2c_0 DY/\alpha_i}$.

We used our model to simulate the development of two biofilms, which grow at rates α_1 and α_2, respectively, and are coupled using our simplified flow model (Fig. 1 *E* and *F* and *Materials and Methods*). In the first instance, we assume that both biofilms can equally resist detachment, but later this assumption is relaxed. To reduce the number of tunable parameters, we nondimensionalized the coupled differential equations governing the biofilm thicknesses, k_i, to yield four dimensionless parameters: $\alpha^* = \alpha_2/\alpha_1$, the ratio of growth rate of the two biofilms; $\beta^* = \sqrt{3\mu Q_T \chi^2/4BL^2\alpha_1^2}$, the strength of flow-induced detachment normalized by the growth rate of the slower-growing biofilm; $\delta^* = \sqrt{2c_0 DY/\alpha_1 L^2}$, the nondimensional growing edge thickness of the slower-growing biofilm; and $M^* = M/L$, the strength of the hydrodynamic coupling between the two biofilms. We initialized each pore with a thin biofilm layer ($k_i/L = 0.01$), which assumes that both strains can initially adhere to surfaces equally well, and then we calculated the thicknesses of the two biofilms until they reached steady state. To isolate how the relative strength of the flow affected the biofilms, we fixed $\delta^* = 0.3$ and $M^* = 1$ to focus our attention on the $[\alpha^*, \beta^*]$ phase plane.

Our model predicted a diversity of different ecological outcomes (Fig. 3 and Fig. S4). When flow was relatively weak ($\beta^* < 0.8$), biofilm growth dominated detachment, such that the positive feedback between increased flow diversion and reduced detachment ultimately led to both biofilms fully blocking their pore spaces (regime c). In the opposite limit, when flow was relatively strong ($\beta^* \gtrsim 1.4$), detachment dominated the growth of the slower-growing biofilm, which was completely scoured away from the surface. In this case, the faster-growing genotype either fully detached (regime a), reached a steady equilibrium thickness (regime d), or blocked its own pore entirely (regime e), depending on the asymmetry in growth rates, α^*. When the flow was at an intermediate level ($\beta^* \approx 0.8$ to 1.4), two outcomes were possible, depending upon the value of α^*: if genotypes grew at a similar rate ($\alpha^* \approx 1$), the fast-growing biofilm initially diverted flow away from its own pore space. However, as the thickness of slower-growing biofilm increased over time, it diverted flow back toward the faster strain, and this stabilizing effect allowed both strains to access flow and disperse cells downstream at steady state, with the faster-growing biofilm dispersing at a larger rate (regime b in Fig. 3; see also Fig. S4). If the asymmetry in the growth rates of the two strains was larger in this intermediate flow regime, the slower-growing strain was not able to stabilize the runaway growth of its neighbor and the faster-growing genotype blocked its pore space (regime f in Fig. 3). Using the biofilm's dispersal rate at steady state, W (equivalent to the rate at which new biofilm is formed at steady state) as an objective measure of fitness, our model indicates that slower-growing biofilms are favored when flow is relatively weak, whereas faster-growing biofilms are favored when flow is relatively strong. We note that our model assumes that cell dispersal is caused purely

by flow-induced detachment and that bacteria do not actively regulate their propensity to detach.

The results from the model are in broad agreement with the two distinct flow regimes observed in our microfluidic experiments, which show that the wild-type biofilm growth tends to reduce its access to flow at smaller flow rates (equivalent to smaller β^*; regime f in Fig. 3) but is able to maintain access to flow at larger flow rates (equivalent to larger β^*; regime b in Fig. 3). Although we could not directly measure rates of cell dispersal in our experiments, we combined our experimental data with a mechanistic model to predict how dispersal rate of each genotype changes over the course of our microfluidic experiments. First, we developed a model to translate the position of the dye interface h_D into the volumetric flow rates q_i that pass through either arm of the device. This information was then combined with measurements of the biofilm thicknesses, k_i, to estimate the shear stress, τ_i, acting on the surface of either biofilm. Finally, both τ_i and k_i were used as inputs in the model of flow-induced biofilm detachment explained above (see *SI Text* for details). This analysis shows that in the high-flow-rate treatment ($Q_T = 2$ mL h^{-1}), both biofilms gradually increase their dispersal rate until beginning to plateau after approximately 40 h (Fig. S5). In contrast, in the low-flow treatment ($Q_T = 0.1$ mL h^{-1}), the wild-type biofilm rapidly increases its dispersal rate until it begins to divert its flow supply, which then causes a precipitous decrease in dispersal (Fig. S5). Although the dye interface cannot be measured once the $\Delta rpoS$ flow path has captured $\approx$95% of the flow (owing to the diffusion of the dye) (*SI Text*), by this point, our analysis predicts that dispersal rate of the wild-type biofilm has already dropped nearly threefold from its peak value. During the same time period, the $\Delta rpoS$ biofilm is predicted to sharply increase its rate of dispersal as it takes on the extra flow from the wild-type biofilm. Although we cannot predict how the two genotypes differ in their rate of dispersal (*SI Text*), this analysis indicates that flow diversion can dramatically affect a biofilm's capacity to shed cells downstream.

The Impact of Flow on the Evolution of Bacterial Growth Rate. Our model shows that a biofilm's fate depends not only on its growth rate but also on the behavior of other biofilms elsewhere within the porous network. However, how do hydrodynamic interactions between genotypes impact bacterial evolution? Over evolutionary timescales, it is expected that biofilm patches will repeatedly form and dissipate as a result of both natural processes and human intervention [e.g., predation (56, 57), enzymatic decay (58), and the periodic flushing of a porous filtration systems (59)]. This continual turnover of biofilm patches means that if new genotypes are introduced into a network of pore spaces—whether through in situ mutation or immigration—then they will be able to form new patches and potentially compete with the resident genotype over many iterated rounds of competition. Our model can then be used as a tool to measure the competitive ability of a newly introduced genotype, allowing us to infer how its frequency will change in the population over time.

To resolve how the bacterial growth rate would evolve over many successive rounds of competition, we embedded our mechanistic model of flow–biofilm interaction within a game theoretical framework known as adaptive dynamics (60). Specifically, this invasion analysis tests whether a novel genotype that grows at rate α_M will be able to increase in frequency and ultimately supplant a population of biofilms that grow at rate α_R based on their relative fitness (*Materials and Methods*). Because the ability of a biofilm to seed new patches is expected to increase with its rate of dispersal, we again use dispersal as a metric to quantify evolutionary fitness. A matrix of different α_R and α_M values is used to construct a so-called pairwise invasibility plot (Fig. 4 and ref. 60), which systematically delineates the growth rates for which a novel mutant can invade and displace the resident population. This representation then allows a generalized

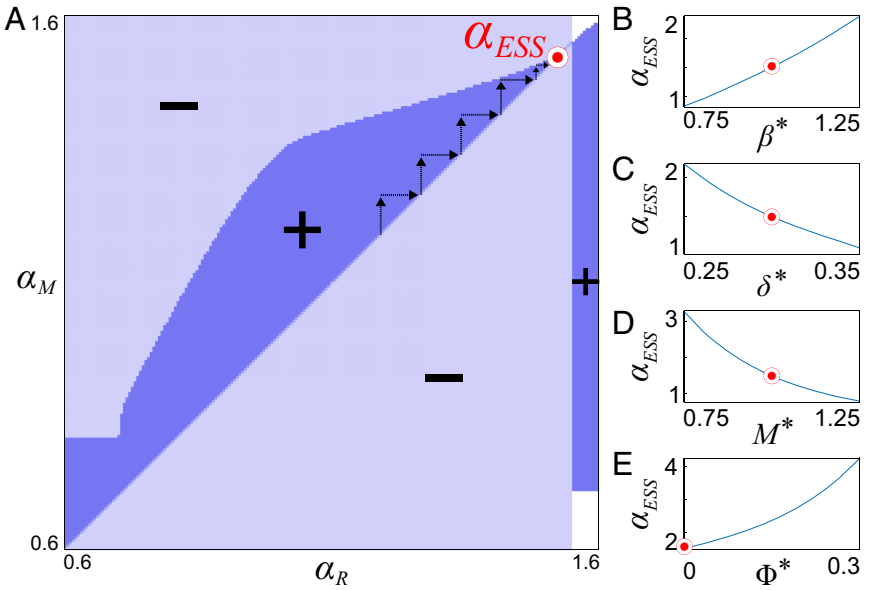

Fig. 4. A game-theoretical analysis of the coupled biofilm model predicts an evolutionary stable growth rate. (*A*) We used adaptive dynamics to construct a pairwise invasion plot, which maps the region of parameter space where a mutant that grows at rate α_M can invade a resident population of biofilms that grows at rate α_R. The mutant can invade in the dark blue regions (+) and cannot invade in the light blue regions (−). In the white regions, the mutant and the resident biofilms both have a fitness of zero ($W_i = 0$) because they have either been fully detached by flow or have blocked their pore space. Arrows show an example evolutionary trajectory where mutant genotypes successively replace the resident population, driving the growth rate toward the evolutionary stable growth rate, α_{ESS} (red circle). Here, we set $\delta^* = 0.3\alpha_R^{-1/2}$ and $\beta^* = 1.1\alpha_R^{-1}$, $M^* = 1$, and $\Phi^* = 0$. (*B–E*) To determine the effect of β^*, δ^*, M^*, and Φ^* on α_{ESS}, we held three of these parameters constant and varied the fourth (red circles show fixed values).

way to infer the trajectory of a population's growth rate over evolutionary timescales (60).

We find that mutants can invade only when their growth rate is slightly larger than the resident population (Fig. 4*A*). However, over time, successive invasions (Fig. 4*A*, arrows) of new genotypes are predicted to systematically increase the growth rate of the resident population until it reaches a evolutionary stable value, α_{ESS}, after which, no new genotypes will be able to invade (Fig. 4*A*). Intuitively, when a biofilm that grows at α_{ESS} competes against a faster-growing strain, the latter will block its pore space. Conversely, when a biofilm that grows at α_{ESS} competes against a slower-growing strain, the latter will disperse fewer cells downstream at steady state. We resolve how α_{ESS} varies as a function of the environmental conditions (Fig. 4 *B*–*D*). Increasing β^*—for example, by increasing the total flow rate—leads to a larger α_{ESS}, while increasing the nondimensional growing edge thickness δ^*—as can occur when nutrients are more plentiful—leads to a smaller α_{ESS}. Moreover, the connectivity of the porous structure also influences this process: increasing M^*, which increases the ability of flow to bypass the focal biofilms, leads to a reduction in α_{ESS}. All of these trends are consistent with the idea that increasing the potential for blocking, whether through lower flow rates, increased growing layer thickness, or an increased ability for flow to divert around competing biofilms, would promote the evolution of slower-growing genotypes. These results suggest that pore blocking places a fundamental physical limitation on the evolution of bacterial growth rates in porous environments and stand in stark contrast with that observed in typical laboratory assays, such as within liquid batch cultures or chemostats, where evolution selects for the fastest-growing genotype (16, 61).

Accounting for Potential Covariance Between Rates of Bacterial Growth and Flow-Induced Detachment Does Not Qualitatively Affect Our Predictions. Our analyses above assume that a biofilm's growth rate can vary independently from its other phenotypic characteristics. However, previous experiments have shown that faster-growing biofilms are more susceptible to flow-induced detachment (62–65). This dependency may occur because fast-growing genotypes invest less in secretions of exopolymeric substances that glue cells together (63) or because rapidly growing genotypes form biofilms with more fragile morphologies, rendering them more susceptible to detachment (55, 66). To model how covariance between growth and detachment influences bacterial competition, we extended our model using the parameterization of Speitel and DiGiano (62), who empirically quantified this coupling in porous environments using radiolabeled carbon sources. This parameterization measures the strength of the coupling between growth and detachment with the nondimensional parameter Φ^* (*SI Text* and refs. 55 and 62): although our initial simulations (Fig. 3) assume $\Phi^* = 0$, a larger Φ^* indicates a stronger coupling between these two processes. Intuitively, a larger Φ^* reduces the potential that a genotype will block its pore space. Whereas the inclusion of this new dependency changes the locations of the various competitive regimes in the $[\alpha^*, \beta^*]$ phase plane, their positions with respect to one another qualitatively remain the same (Fig. S6 and *SI Text*). Thus, the conclusions from our original model ($\Phi^* = 0$), namely that faster-growing genotypes are favored when flow is rapid but are selected against when flow is weak, are robust to this additional dependency. Moreover, the inclusion of this additional term in our game-theoretical model reveals that a smaller Φ^* leads to a reduction in the predicted α_{ESS}, which is again consistent with the idea that increasing the potential for blocking reduces the evolutionary stable growth rate (Fig. 4*E*). Although it is possible that other phenotypic interdependencies could qualitatively affect microbial competition and evolution, these results indicate that the conclusions of our initial model still hold when a dependency between growth and detachment is included.

Discussion

Biofilms growing in porous environments facilitate a wide range of important processes in the natural environment and industry (8, 24–26, 67–71). Our proof-of-principle experiments, mathematical modeling, and game-theoretical analyses show that the feedback between biofilm proliferation and porous media hydrodynamics can dramatically affect how different genotypes compete. We find that relatively strong and weak flow conditions favor fast- and slow-growing biofilms, respectively, whereas intermediate flow rates allow biofilms with different growth rates to maintain access to flow (Fig. 3).

In industrial settings, these principles could be exploited to engineer microbial systems to favor a bacterial species with a particular growth rate or keep multiple species with different growth rates active over longer time scales. For example, in porous wastewater reactors, relatively fast-growing species of bacteria convert ammonia to nitrite, but it is desirable to inhibit often slower-growing species that further oxidize these products into nitrate, a potent environmental contaminant (72). Our work predicts then that using a larger flow rate may be a way to favor the former species of bacteria over the latter. In contrast, the remediation of mercury-contaminated wastewater in porous reactors can be enhanced by maintaining multiple species of bacteria that grow at different rates (73). Moreover, our findings suggest that inoculating porous substrates with a community of cells from the effluent of a porous system would favor the growth of biofilms that do not block their pore space, whereas inoculating cells from communities that have evolved in homogeneous laboratory conditions would promote blocking. Such information has implications for the design of effective water treatment systems, where blocking reduces efficiency, or in the design of biobarriers to stifle the movement of groundwater contaminants, where blocking is the main objective.

Our results may also shed light on how cells compete in natural environments. We expect that temporal fluctuations in flow and heterogeneity in pore size will promote diversity. This variablity is expected to be common due to episodic patterns of rainfall and geological processes that mix different particle sizes (74). However, some groundwater aquifers and packed-bed bioreactors have nearly constant rates of flow and a more uniform distribution of pore spaces, which may promote competitive exclusion. In systems where blocking does occur, natural selection may favor cells periodically detaching en masse to regain access to flow. Broadly consistent with this hypothesis, increased detachment has been observed empirically in response to nutrient deprivation and quorum sensing (75, 76).

Bacteria are the subject of intense empirical and theoretical study. However, the vast majority of work on bacteria focuses on their behavior in liquid cultures or in simple biofilm assays. Here, we have combined diverse bodies of theory, including fluid dynamics and game theory, to understand how bacteria compete and evolve within the complex porous environments where most bacteria live. Our assumptions greatly simplify the complexity of these systems, so there is considerable potential for extensions to our work. Many microbial traits can influence biofilm formation, including the strength of initial cell adhesion, which may itself be a function of the hydrodynamic or nutrient conditions (21, 77), production of extracellular polysaccharides (78), streamer formation (30, 79), quorum sensing (80), motility (81), and cell metabolism (82, 83). Further work will be needed to resolve how the wide diversity of microbial traits impact the processes described here.

Future efforts will also be required to resolve how the specific structure of the pore space and the distribution of different genotypes within them affect microbial competition. While our work

predicts that bacteria can benefit from making less biofilm when growing in a clonal patch, this may change in mixed-genotype biofilms, where the priority may shift to locally outgrowing competitors (84). It is interesting, then, that bacteria are known to respond to competing strains by increasing their investment into biofilm (85).

In sum, our approaches indicate that porous habitats, and the flows within them, can have a profound impact on bacterial evolution. Although rapid division gives a microbe an evolutionary advantage in typical laboratory environments, our results suggest that this paradigm does not extend to many bacterial habitats.

Materials and Methods

Modeling Stokes Flow Through a Representative Network of Pore Spaces. The geometry of the pore space (Fig. 1 *A*–*C*) was obtained using Particle Flow Code in Two Dimensions (Itasca), which models the mechanical processes that form many porous substrates. The particle locations were then imported into COMSOL Multiphysics to model incompressible Stokes flow within the pore spaces between the particles using the finite element method. Zero-flux, no-slip boundary conditions were used at the left and right boundaries of the computational domain as well as on the surfaces of all of the particles. At the top and bottom boundaries of the computational domain, the pressure was fixed at two different values, such that the resulting pressure gradient was responsible for driving flow. The Stokes equations were solved with and without the presence of a biofilm patch in one of the pore spaces. Results were then exported into Matlab 2015a (MathWorks) for further analysis and plotting.

Bacterial Strains and Culturing. Our experiments used *E. coli* strain K12-W3110 and a mutant with a rpoS819 allele insertion (86, 87). Each strain was labeled with either green fluorescent protein (GFP) or red fluorescent protein (RFP). Cell cultures were grown overnight in tryptone broth (1× TB) (10 g of Bacto Tryptone per 1 L of water) at 37°C, diluted to an optical density of 0.1 (at 600 nm), and then grown for a further hour at 37°C so that cells were in exponential phase when they were first introduced into the microfluidic devices.

Competition Experiments. Microfluidic device masters were fabricated from SU-8 on silicon wafers using standard soft lithography techniques (88) and were cast with polydimethylsiloxane (PDMS) (Sylgard 184; Dow Corning). The depth of these devices was $2B = 75$ μm (Fig. S1). Cured PDMS was bonded to glass coverslips (50 mm × 75 mm; no. 1.5 thickness; Agar Scientific) with a corona discharge system (BD-20AC; Electro-Technic Products) using previously described techniques (89). Tygon tubing (0.51-mm inner radius; Microbore) was used to plumb the inlets and outlets of the device.

For the high-flow-rate treatments ($Q_T = 2$ mL h^{-1}), the outlet was connected to a 140 mL syringe (Harvard Apparatus), which was mounted on a Harvard Apparatus PhD 2000 syringe pump. In the low-flow treatments ($Q_T = 0.1$ mL h^{-1}), the outlet was connected to a 20-mL syringe (Becton Dickinson) mounted on a Harvard Apparatus PhD Ultra syringe pump.

After the microfluidic device and tubing were primed with 1× TB to remove air from the system, cells were introduced into the device by pulling cultures of the wild-type and Δ*rpoS* mutant cells through the device at $Q_T = 0.1$ mL h^{-1}. Unlike many biofilm experiments, where cells are allowed to attach to surfaces in the absence of flow (e.g., refs. 17, 90, 91), we inoculated cells under flow to help keep the two strains confined to their respective pore spaces. Cultures of the wild-type and Δ*rpoS* mutant were simultaneously drawn through the device for 20 h to allow cells to attach and then we switched over to withdrawing tryptone broth (0.5× TB) (5 g of tryptone per liter of water) through the device for a further 48 h so that a thin biofilm was established in each of the pore spaces. We initiated the biofilms in the high- and low-flow treatments in the same way in the first 3 d of the experiment to ensure that the cell attachment was similar between the two treatments. After this initial inoculation phase, we connected one of the inlets of the device to a reservoir containing tryptone broth (0.5× TB) mixed with dye (Chicago Blue; Sigma Aldrich) that enabled us to dynamically track the relative proportion of flow passing through each side of the device.

After the initial inoculation phase, we applied a flow rate of $Q_T = 2$ mL h^{-1} in the high-flow-rate treatment, whereas in the low-flow-rate treatment, we used a flow rate of $Q_T = 0.1$ mL h^{-1}. We imaged the devices every 30 min for the next 70 h, which allowed both treatments to reach a steady state. Each treatment was repeated three times, and each yielded the same result at steady state (Fig. S3). The time points shown in Fig. 2 and Figs. S3 and S5 are measured from the end of the inoculation phase.

Mechanistic Model of Biofilm Competition. Our mathematical model of biofilm competition simulates the two processes that are predicted to dominate biofilm development in flowing environments: bacterial growth and the flow induced detachment (45, 52). The differential equations that govern the thicknesses of the two biofilms k_i (Eq. **1**) are hydrodynamically coupled using an approach that is widely used for low Reynolds number flows (92). Specifically, we consider three flow paths of equal length connected in parallel, so the total volumetric flow rate, Q_T, divides among the three pathways as a function of their hydrodynamic resistances, R_i. Poiseuille's law states that $q_i = dP/R_i$, where q_i is the flow rate along each path, $-dP$ is the drop in pressure across the system, and $R_i = 3\mu/4B(L-k_i)^3$ is the hydrodynamic resistance per unit length of each flow path, where μ is the dynamic velocity of the fluid, $2B$ is the span wise dimension of the pore space, $2L$ is the pore width and $L \ll B$.

All three flow paths experience the same difference in pressure, $dP = Q_T R_T$, which is determined by the effective resistance of the entire system, R_T, where (92)

$$\frac{1}{R_T} = \frac{1}{R_1} + \frac{1}{R_2} + \frac{1}{R_3}. \quad [2]$$

Solving for dP and substituting into the equation for q_i yields

$$q_i = \frac{Q_T}{R_i}\frac{1}{1/R_1 + 1/R_2 + 1/R_3}, \quad [3]$$

which, can then be written in terms of the biofilm thicknesses,

$$q_i = Q_T \frac{(L-k_i)^3}{(L-k_1)^3 + (L-k_2)^3 + M^3}. \quad [4]$$

This expression conserves flow, so that $Q_T = q_1 + q_2 + q_3$. We note that the approach used here is analogous to that routinely used in the analysis of electric circuits (92).

Our equation for hydrodynamic resistance assumes pressure-driven, planar flow between two parallel plates separated by a distance $2(L-k_i)$, where the velocity profile in the ith channel is given by $u(y) = \frac{dP}{2\mu}(y^2 - (L-k_i)^2)$ and y is the distance from the centerline of the channel. Thus, the hydrodynamic shear stress acting on the biofilm is given by

$$\tau = \mu\frac{du}{dy} = \frac{3\mu q_i}{4B(L-k_i)^2}, \quad [5]$$

where du/dy has been evaluated at the biofilm's surface, $y = L - k_i$.

Combining Eqs. **1**, **4**, and **5** yields the coupled differential equations that govern k_1 and k_2, the thicknesses of the two biofilms:

$$\frac{dk_1}{dt} = \alpha_1 \min(\delta_1, k_1) - k_1\sqrt{\frac{3\mu Q_T \chi^2}{4B}}\sqrt{\frac{(L-k_1)}{(L-k_1)^3 + (L-k_2)^3 + M^3}}, \quad [6]$$

$$\frac{dk_2}{dt} = \alpha_2 \min(\delta_2, k_2) - k_2\sqrt{\frac{3\mu Q_T \chi^2}{4B}}\sqrt{\frac{(L-k_2)}{(L-k_1)^3 + (L-k_2)^3 + M^3}}. \quad [7]$$

We nondimensionalized the governing equations above using the pore half-width L as our characteristic length scale and the reciprocal growth rate of strain 1, $1/\alpha_1$, as our characteristic time scale, such that $k_1 = Lk_1^*$, $k_2 = Lk_2^*$, $M = LM^*$, and $t = t^*/\alpha_1$. We obtain the dimensionless equations

$$\frac{dk_1}{dt} = \min(k_1, \delta^*) - \beta^* k_1\sqrt{\frac{(1-k_1)}{\theta}}, \quad [8]$$

$$\frac{dk_2}{dt} = \alpha^* \min\left(k_2, \frac{\delta^*}{\sqrt{\alpha^*}}\right) - \beta^* k_2\sqrt{\frac{(1-k_2)}{\theta}}, \quad [9]$$

$$\text{where } \theta = (1-k_1)^3 + (1-k_2)^3 + (M^*)^3, \quad [10]$$

where we have omitted the asterisks from k_i and t for clarity. These equations were solved numerically using Matlab. Specifically, we initialized two pore spaces with a thin layer of biofilm, $k_1 = k_2 = 0.01$, similar to the initially sparse seeding of cells in our experiments (Fig. 2 and *Materials and Methods*, *Competition Experiments*) and then integrated the dimensionless equations until each biofilm had converged to a steady state thickness.

Game Theoretical Analysis. To examine how hydrodynamic interactions impact biofilm evolution, we embedded the mechanistic model presented above within an adaptive dynamics framework (60, 93). This analysis examines whether a new genotype is able to invade and displace a porous environment already colonized by "resident" genotype. Specifically, adaptive dynamics assumes that the rate at which novel genotypes are introduced into a group of interacting pore spaces—either through in situ mutation or immigration—is small compared with the rate at which a new genotype can displace the resident population (94). This assumption means that we can consider the pairwise interaction of a novel genotype that grows at α_M with a monomorphic resident population growing at α_R.

We assumed that the fitness of a genotype is directly proportional to its rate of cell dispersal at steady state, which is equal to the rate of biofilm growth at steady state (Eq. **1**). In our model, the fitness of a biofilm, W, is a function of its growth rate, its competitor's growth rate, and the properties of the pore space (Fig. 3). Two conditions must then hold for a "mutant" to supplant the resident genotype. First, the fitness of the mutant when competing against the resident, denoted $W(\alpha_M, \alpha_R)$, must be larger than or equal to that of the resident competing against itself, $W(\alpha_R, \alpha_R)$. This condition tests whether an initially rare mutant is able to gradually increase in frequency within the population. Second, the fitness of the resident when competing against the mutant, $W(\alpha_R, \alpha_M)$, must be smaller than that of the mutant competing against itself $W(\alpha_M, \alpha_M)$. This condition tests whether the original resident growth strategy will be able to reinvade the system once the mutant has increased in frequency. More formally, the following two criteria must hold for a mutant to invade a resident population:

$$W(\alpha_M, \alpha_R) \geq W(\alpha_R, \alpha_R), \quad [11]$$

$$W(\alpha_R, \alpha_M) < W(\alpha_M, \alpha_M). \quad [12]$$

These criteria are then used to construct a pairwise invasibility plot (Fig. 4 and ref. 60), which can be used to infer the evolutionary trajectory of the population's growth rate.

ACKNOWLEDGMENTS. We thank Juan Keymer for bacterial strains. K.Z.C. was funded by the Engineering and Physical Sciences Research Council, K.R.F. was funded by European Research Council Grant 242670, and W.M.D. was funded by Human Frontier Science Program Fellowship LT001181/2011L.

1. Azam F, Malfatti F (2007) Microbial structuring of marine ecosystems. *Nat Rev Microbiol* 5(10):782–791.
2. Schluter J, Foster KR (2012) The evolution of mutualism in gut microbiota via host epithelial selection. *PLoS Biol* 10(11):e1001424.
3. Bever JD, Richardson SC, Lawrence BM, Holmes J, Watson M (2009) Preferential allocation to beneficial symbiont with spatial structure maintains mycorrhizal mutualism. *Ecol Lett* 12(1):13–21.
4. Horner-Devine MC, Carney KM, Bohannan BJM (2004) An ecological perspective on bacterial biodiversity. *Proc Biol Sci* 271(1535):113–122.
5. Franzosa EA, et al. (2015) Sequencing and beyond: Integrating molecular 'omics' for microbial community profiling. *Nat Rev Microbiol* 13(6):360–372.
6. Allen EE, Banfield JF (2005) Community genomics in microbial ecology and evolution. *Nat Rev Microbiol* 3(6):489–498.
7. Rusconi R, Garren M, Stocker R (2014) Microfluidics expanding the frontiers of microbial ecology. *Annu Rev Biophys* 43(1):65–91.
8. Whitman WB, Coleman DC, Wiebe WJ (1998) Prokaryotes: The unseen majority. *Proc Natl Acad Sci USA* 95(12):6578–6583.
9. Ghiorse WC, Wilson JT (1988) Microbial ecology of the terrestrial subsurface. *Adv Appl Microbiol* 33:107–172.
10. Torsvik V, Øvreås L, Thingstad TF (2002) Prokaryotic diversity–magnitude, dynamics, and controlling factors. *Science* 296(5570):1064–1066.
11. Rothman DH, Forney DC (2007) Physical model for the decay and preservation of marine organic carbon. *Science* 316(5829):1325–1328.
12. Moons P, Michiels CW, Aertsen A (2009) Bacterial interactions in biofilms. *Crit Rev Microbiol* 35(3) :157–168.
13. Xavier JB, Foster KR (2007) Cooperation and conflict in microbial biofilms. *Proc Natl Acad Sci USA* 104(3):876–881.
14. Nadell CD, Xavier JB, Levin SA, Foster KR (2008) The evolution of quorum sensing in bacterial biofilms. *PLoS Biol* 6(1):e14.
15. Rao D, Webb JS, Kjelleberg S (2005) Competitive interactions in mixed-species biofilms containing the marine bacterium *Pseudoalteromonas tunicata*. *Appl Environ Microbiol* 71(4):1729–1736.
16. Hibbing ME, Fuqua C, Parsek MR, Peterson SB (2010) Bacterial competition: Surviving and thriving in the microbial jungle. *Nat Rev Microbiol* 8(1):15–25.
17. Klausen M, et al. (2003) Biofilm formation by *Pseudomonas aeruginosa* wild type, flagella and type IV pili mutants. *Mol Microbiol* 48(6):1511–1524.
18. Kim W, Racimo F, Schluter J, Levy SB, Foster KR (2014) Importance of positioning for microbial evolution. *Proc Natl Acad Sci USA* 111(16):E1639–E1647.
19. Stoodley P, et al. (2001) Growth and detachment of cell clusters from mature mixed-species biofilms. *Appl Environ Microbiol* 67(12):5608–5613.
20. Chambless JD, Stewart PS (2007) A three-dimensional computer model analysis of three hypothetical biofilm detachment mechanisms. *Biotechnol Bioeng* 97(6): 1573–1584.
21. Zhang W, Sileika T, Packman AI (2013) Effects of fluid flow conditions on interactions between species in biofilms. *FEMS Microbiol Ecol* 84(2):344–354.
22. Thullner M (2010) Comparison of bioclogging effects in saturated porous media within one- and two-dimensional flow systems. *Ecol Eng* 36(2):176–196.
23. Cunningham AB, Sharp RR, Hiebert R, James G (2003) Subsurface biofilm barriers for the containment and remediation of contaminated groundwater. *Bioremediat J* 7(3-4):151–164.
24. Raiders RA, Knapp RM, McInerney MJ. (1989) Microbial selective plugging and enhanced oil recovery. *J Ind Microbiol Biotechnol* 4(3) :215–229.
25. Nicolella C, van Loosdrecht MC, Heijnen JJ (2000) Wastewater treatment with particulate biofilm reactors. *J Biotechnol* 80(1):1–33.
26. Kim JW, Choi H, Pachepsky YA (2010) Biofilm morphology as related to the porous media clogging. *Water Res* 44(4):1193–1201.
27. Cunningham AB, Characklis W, Abedeen F, Crawford D (1991) Influence of biofilm accumulation on porous media hydrodynamics. *Environ Sci Technol* 25(7): 1305–1311.
28. Shafahi M, Vafai K (2009) Biofilm affected characteristics of porous structures. *Int J Heat Mass Tran* 52(3-4):574–581.
29. Graf von der Schulenburg DA, Pintelon TRR, Picioreanu C, Van Loosdrecht MCM, Johns ML (2009) Three-dimensional simulations of biofilm growth in porous media. *AIChE Journal* 55(2):494–504.
30. Drescher K, Shen Y, Bassler BL, Stone HA (2013) Biofilm streamers cause catastrophic disruption of flow with consequences for environmental and medical systems. *Proc Natl Acad Sci USA* 110(11):4345–4350.
31. Dupin HJ, Kitanidis PK, McCarty PL (2001) Pore-scale modeling of biological clogging due to aggregate expansion: A material mechanics approach. *Water Resour Res* 37(12):2965–2979.
32. Nadell CD, Foster KR, Xavier JB (2010) Emergence of spatial structure in cell groups and the evolution of cooperation. *PLoS Comput Biol* 6(3):e1000716.
33. Millet YA, et al. (2014) Insights into *Vibrio cholerae* intestinal colonization from monitoring fluorescently labeled bacteria. *PLoS Pathog* 10(10):e1004405.
34. Mitri S, Foster KR (2013) A genotypic view of social interactions in microbial communities. *Annu Rev Genet* 47:265–291.
35. Hallatschek O, Hersen P, Ramanathan S, Nelson DR (2007) Genetic drift at expanding frontiers promotes gene segregation. *Proc Natl Acad Sci USA* 104(50): 19926–19930.
36. van Gestel J, Weissing FJ, Kuipers OP, Kovács AT (2014) Density of founder cells affects spatial pattern formation and cooperation in *Bacillus subtilis* biofilms. *ISME J* 8(10):2069–2079.
37. Pintelon TRR, Graf von der Schulenburg DA, Johns ML (2009) Towards optimum permeability reduction in porous media using biofilm growth simulations. *Biotechnol Bioeng* 103(4):767–779.
38. Adams JL, McLean RJ (1999) Impact of *rpoS* deletion on *Escherichia coli* biofilms. *Appl Environ Microbiol* 65(9):4285–4287.
39. Ito A, May T, Kawata K, Okabe S (2008) Significance of *rpoS* during maturation of *Escherichia coli* biofilms. *Biotechnol Bioeng* 99(6):1462–1471.
40. Trulear MG, Characklis WG (1982) Dynamics of biofilm processes. *Water Pollut Control Fed* 54(9):1288–1301.
41. Stoodley P, Cargo R, Rupp CJ, Wilson S, Klapper I (2002) Biofilm material properties as related to shear-induced deformation and detachment phenomena. *J Ind Microbiol Biotechnol* 29(6):361–367.
42. Stewart PS (1993) A model of biofilm detachment. *Biotechnol Bioeng* 41(1):111–117.
43. Donlan RM (2002) Biofilms: Microbial life on surfaces. *Emerg Infect Dis* 8(9):881–890.
44. van Loosdrecht MCM, et al. (1995) Biofilm structures. *Water Sci Tech* 32(8):35–43.
45. Duddu R, Chopp DL, Moran B (2009) A two-dimensional continuum model of biofilm growth incorporating fluid flow and shear stress based detachment. *Biotechnol Bioeng* 103(1):92–104.
46. Williamson K, McCarty PL (1976) A model of substrate utilization by bacterial films. *J Water Pollut Control Fed* 48(1):9–24.
47. Werner E, et al. (2004) Stratified growth in *Pseudomonas aeruginosa* biofilms. *Appl Environ Microbiol* 70(10):6188–6196.
48. Pirt S (1967) A kinetic study of the mode of growth of surface colonies of bacteria and fungi. *J Gen Microbiol* 42(2):181–197.
49. Horn H, Lackner S (2014) Modeling of biofilm systems: A review. *Adv Biochem Eng Biotechnol* 146:53–76.
50. Rittmann B (1982) The effect of shear stress on biofilm loss rate. *Biotechnol Bioeng* 24(2):501–506.
51. Abbas F (2011) Mathematical contributions to one-dimensional biofilm modeling. PhD thesis (University of Guelph, Guelph, Canada).
52. Abbas F, Sudarsan R, Eberl HJ (2012) Longtime behavior of one-dimensional biofilm models with shear dependent detachment rates. *Math Biosci Eng* 9(2):215–239.
53. Wanner O, Gujer W (1986) A multispecies biofilm model. *Biotechnol Bioeng* 28: 314–328.
54. Brovelli A, Malaguerra F, Barry DA (2009) Bioclogging in porous media: Model development and sensitivity to initial conditions. *Environ Model Software* 24(5): 611–626.
55. Ebigbo A, Helmig R, Cunningham AB, Class H, Gerlach R (2010) Modelling biofilm growth in the presence of carbon dioxide and water flow in the subsurface. *Adv Water Resour* 33(7):762–781.

56. Lawrence J, Scharf B, Packroff G, Neu TR (2002) Microscale evaluation of the effects of grazing by invertebrates with contrasting feeding modes on river biofilm architecture and composition. *Microb Ecol* 44(3):199–207.
57. DeLeo PC, Baveye P (1997) Factors affecting protozoan predation of bacteria clogging laboratory aquifer microcosms. *Geomicrobiol J* 14(2):127–149.
58. Allison DG, Ruiz B, SanJose C, Jaspe A, Gilbert P (1998) Extracellular products as mediators of the formation and detachment of *Pseudomonas fluorescens* biofilms. *FEMS Microbiol Lett* 167(2):179–184.
59. Moreira M, Feijoo G, Palma C, Lema J (1997) Continuous production of manganese peroxidase by *Phanerochaete chrysosporium* immobilized on polyurethane foam in a pulsed packed-bed bioreactor. *Biotechnol Bioeng* 56(2):130–137.
60. Brännström Å, Johansson J, von Festenberg N (2013) The hitchhiker's guide to adaptive dynamics. *Games* 4(3):304–328.
61. Ibarra RU, Edwards JS, Palsson BO (2002) *Escherichia coli* K-12 undergoes adaptive evolution to achieve in silico predicted optimal growth. *Nature* 420(6912):186–189.
62. Speitel GE, DiGiano FA (1987) Biofilm shearing under dynamic conditions. *J Environ Eng* 113(21534):464–475.
63. Robinson JA, Trulear MG, Characklis WG (1984) Cellular reproduction and extracellular polymer formation by *Pseudomonas aeruginosa* in continuous culture. *Biotechnol Bioeng* 26(12):1409–1417.
64. Clement TP, Hooker BS, Skeen RS (1996) Macroscopic models for predicting changes in saturated porous media properties caused by microbial growth. *Ground Water* 34(5):934–942.
65. Peyton BM, Characklis W (1993) A statistical analysis of the effect of substrate utilization and shear stress on the kinetics of biofilm detachment. *Biotechnol Bioeng* 41(7):728–735.
66. Picioreanu C, van Loosdrecht MC, Heijnen JJ (2001) Two-dimensional model of biofilm detachment caused by internal stress from liquid flow. *Biotechnol Bioeng* 72(2): 205–218.
67. Danhorn T, Fuqua C (2007) Biofilm formation by plant-associated bacteria. *Annu Rev Microbiol* 61:401–422.
68. De Muynck W, De Belie N, Verstraete W (2010) Microbial carbonate precipitation in construction materials: A review. *Ecol Eng* 36(2):118–136.
69. Mitchell AC, Dideriksen K, Spangler LH, Cunningham AB, Gerlach R (2010) Microbially enhanced carbon capture and storage by mineral-trapping and solubility-trapping. *Environ Sci Technol* 44(13):5270–5276.
70. Leite JAC, Fernandes BS, Pozzi E, Barboza M, Zaiat M (2008) Application of an anaerobic packed-bed bioreactor for the production of hydrogen and organic acids. *Int J Hydrogen Energ* 33(2):579–586.
71. Michalakos GD, Nieva JM, Vayenas DV, Lyberatos G (1997) Removal of iron from potable water using a trickling filter. *Water Res* 31(5):991–996.
72. Cho S, Fujii N, Lee T, Okabe S (2011) Development of a simultaneous partial nitrification and anaerobic ammonia oxidation process in a single reactor. *Bioresour Technol* 102(2):652–659.
73. Von Canstein H, Kelly S, Li Y, Wagner-Döbler I (2002) Species diversity improves the efficiency of mercury-reducing biofilms under changing environmental conditions. *Appl Environ Microbiol* 68(6):2829–2837.
74. Rehfeldt KR, Boggs JM, Gelhar LW (1992) Field study of dispersion in a heterogeneous aquifer: 3. Geostatistical analysis of hydraulic conductivity. *Water Resour Res* 28(12):3309–3324.
75. Kong KF, Vuong C, Otto M (2006) *Staphylococcus* quorum sensing in biofilm formation and infection. *Int J Med Microbiol* 296(2-3):133–139.
76. Sauer K, et al. (2004) Characterization of nutrient-induced dispersion in *Pseudomonas aeruginosa* PAO1 biofilm. *J Bacteriol* 186(21):7312–7326.
77. Lecuyer S, et al. (2011) Shear stress increases the residence time of adhesion of *Pseudomonas aeruginosa*. *Biophys J* 100(2):341–350.
78. Danese PN, Pratt LA, Kolter R (2000) Exopolysaccharide production is required for development of *Escherichia coli* K-12 biofilm architecture. *J Bacteriol* 182(12): 3593–3596.
79. Valiei A, Kumar A, Mukherjee PP, Liu Y, Thundat T (2012) A web of streamers: Biofilm formation in a porous microfluidic device. *Lab Chip* 12(24):5133–5137.
80. Hammer BK, Bassler BL (2003) Quorum sensing controls biofilm formation in *Vibrio cholerae*. *Mol Microbiol* 50(1):101–104.
81. Zhao K, et al. (2013) Psl trails guide exploration and microcolony formation in *Pseudomonas aeruginosa* biofilms. *Nature* 497(7449):388–391.
82. Bjergbæk LA, Haagensen JAJ, Reisner A, Molin S, Roslev P (2007) Effect of oxygen and growth medium on in vitro biofilm formation by *Escherichia coli*. *Biofilms* 3(1):1–10.
83. Colón-González M, Méndez-Ortiz MM, Membrillo-Hernández J (2004) Anaerobic growth does not support biofilm formation in *Escherichia coli* K-12. *Res Microbiol* 155(7):514–521.
84. Nadell CD, Drescher K, Foster KR (2016) Spatial structure, cooperation, and competition in biofilms. *Nat Rev Microbiol* 14:589–600.
85. Oliveira NM, et al. (2015) Biofilm formation as a response to ecological competition. *PLoS Biol* 13(8):e1002232.
86. Keymer JE, Galajda P, Lambert G, Liao D, Austin RH (2008) Computation of mutual fitness by competing bacteria. *Proc Natl Acad Sci USA* 105(51):20269–20273.
87. Lambert G, Liao D, Vyawahare S, Austin RH (2011) Anomalous spatial redistribution of competing bacteria under starvation conditions. *J Bacteriol* 193(8):1878–1883.
88. Whitesides G, Ostuni E, Takayama S, Jiang X, Ingber D (2001) Soft lithography in biology and biochemistry. *Annu Rev Biomed Eng* 3(1):335–373.
89. Haubert K, Drier T, Beebe D (2006) PDMS bonding by means of a portable, low-cost corona system. *Lab Chip* 6(12):1548–1549.
90. Moller S, et al. (1998) In situ gene expression in mixed-culture biofilms: Evidence of metabolic interactions between community members. *Appl Environ Microbiol* 64(2):721–732.
91. Drenkard E, Ausubel FM (2002) *Pseudomonas* biofilm formation and antibiotic resistance are linked to phenotypic variation. *Nature* 416(6882):740–743.
92. Stone HA (2007) Introduction to fluid dynamics for microfluidic flows. Series on Integrated Circuits and Systems, eds Lee H, Westervelt RM, Ham D (Springer, Boston, MA).
93. Diekmann ODO (2004) A beginner's guide to adaptive dynamics. Mathematical Modelling of Population Dynamics, ed Rudnicki R (Banach Center Publications, Warsaw) Vol 63, pp 47–86.
94. Nowak MA, Sigmund K (2004) Evolutionary dynamics of biological games. *Science* 303(5659):793–799.
95. Sinton LW, et al. (2010) Transport of *Escherichia coli* and F-RNA bacteriophages in a 5m column of saturated pea gravel. *J Contam Hydrol* 117(1):71–81.
96. Biggar JW, Nielsen DR (1976) Spatial variability of the leaching characteristics of a field soil. *Water Resour Res* 12(1):78–84.
97. Schindelin J, et al. (2012) Fiji: An open-source platform for biological-image analysis. *Nat Methods* 9(7):676–682.
98. Valko E (1935) Measurements of the diffusion of dyestuffs. *Trans Faraday Soc* 31: 230–245.